SUPPLEMENTARY INFORMATION

From cellular lysis to microarray detection, an integrated thermoplastic elastomer (TPE) point of care Lab on a Disc

Emmanuel Roy,*[a] Gale Stewart,[b] Maxence Mounier,[a] Lidija Malic,[a] Régis Peytavi,[b] Liviu Clime,[a] Marc Madou,[c] Maurice Bossinot,[b] Michel G. Bergeron,[b] and Teodor Veres*[a]

[1]Life sciences Division, National Research Council of Canada, 75 de Mortagne Boulevard, Boucherville, Québec, J4B 6Y, Canada

[2]Centre de Recherche en Infectiologie, Université Laval, 2705 Boul. Laurier, Sainte-Foy, Québec, G1V 4G, Canada,

[3]Department of Mechanical and Aerospace Engineering, University of California, Irvine, CA, USA,

1. Materials and Methods

1.1 Centrifugal microfluidic functions

1.1.1 Capillary valves

Capillary valves offer an attractive approach to regulate the release of liquids on a CD platform. Herein, complementary to previously reported works and theory, we describe and broaden the valve bursting conditions.[1,2] Two main considerations referring to the wetting properties of the liquid versus the surface properties are described. For hydrophilic consideration, a sudden expansion of the microchannel traps the liquid meniscus. The liquid meniscus is stopped at the valve entrance until the driving spinning force overcomes the resisting capillary force. The pertinent dimension and properties which mathematically describe the capillary burst frequency are shown in figure 2a. Herein, we adapted the detailed work of Cho *et al.,*[3] and used their approach based on contact line motion localized at the channel expansion. In addition to their model, we included a mean value for the advancing contact angle which accounted for the different substrate material used to seal the microfluidic channel. We also used a correction factor for the hydraulic diameter to account for the rectangular cross-section of the microfluidic structure.[4] Finally, the burst frequency for the hydrophilic situation can be written as:

$$\omega^2 = \frac{\sigma \sin \overline{\theta_{adv}}}{\pi^2 \rho \Delta r \bar{r} D_h^{1.14}} \qquad (1)$$

Where ω, σ, ρ are respectively the angular velocity, the surface energy and the liquid density, Δr and $\bar{r}$ are respectively the radial length occupied by the liquid, and the average distance of the liquid element versus CD center. D_h refers to the hydraulic diameter and describes a rectangular channel section of a width and height (w,h) equivalent to a cylindrical channel having a D_h diameter.

$$D_h = \frac{4wh}{2w + 2h} \qquad (2)$$

Finally, $\bar{\theta}_{adv}$, is a balanced value of the different advancing contact angles.

$$\overline{\theta_{adv}} = \frac{w}{2w+2h}\theta_{adv,sub} + \frac{w+2h}{2w+2h}\theta_{adv,channel} \quad (3)$$

$\theta_{adv,channel}$ and $\theta_{adv,sub}$ are respectively the advancing contact angles with the microfluidic part, and the sealing substrate. Finally, if $\overline{\theta_{adv}} \geq \pi/2$, the bursting condition described in equation (1) is expressed in the same manner with the term $\sin \theta_{adv}^{-}$ fixed to 1.

Hydrophobic valve situation featured a sudden decrease in the channel cross-section, preventing the liquid to flow downstream. The required pressure to overcome the narrowing effect and to force the liquid to penetrate the channel can be described using the equation (4). Figure 3a illustrates this situation, and a pure geometrical consideration allows the calculation of the capillary force required for the liquid to flow through the valve. Same considerations regarding D_h and the balanced contact angle θ_{adv}^{-} have been taken into account.

$$\omega^2 = \frac{\sigma \cos(\pi - \overline{\theta_{adv}})}{\pi^2 \rho \Delta r \bar{r} D_h^{1.14}} \quad (4)$$

Table 1 reports the measured contacts angles of the different liquids and the mixed liquid compositions used for the proposed assay. Table 4 presents the calculated burst frequencies and the corresponding width and height (w,h) values for the valves integrated on the CD.

1.1.2 Flow rate on CD microfluidic

The lack of well-developed analytical tools to describe the steady state flow rate on a CD platform limits the integration of complex on-board protocols requiring numerous liquid handling and time-dependent liquid flow control. In this work, we propose a simple and general approach to treat the control of flow rate on a CD. For a microfluidic circuit consisting of a series of N channels of different cross-sectional areas $S_1, S_2, S_3, \ldots, S_N$ and different lengths $L_1, L_2, \ldots, L_N$ ending at positions r_1, r_2, ..., r_{N+1}, we can write the following integral from Navier-Stokes equation along a single channel i as:

$$\lambda_{hyd} \int_{(C_i)} Q dl = \int_{(C_i)} (-dp) + \int_{(C_i)} f dl \quad (6)$$

where Q is the flow rate of the liquid, dp is the pressure gradient and f is the centrifugal force density. $\lambda_{hyd} = R_{hyd}/L$ is a linear density related to the amount of hydraulic resistance per unit length of the channel. Since Q is constant along the channel, the integral in the left hand of Eq. (6) is reduced to QL_i, with L_i being the total length of the channel i. The first term in the right hand is $p_{i-1} - p_i$, whereas the last one represents the work done by the centrifugal field on the liquid in the channel. Consequently, the total flow rate through the microfluidic circuit can be written as:

$$Q = \frac{\frac{1}{2}\rho\omega^2\left(r_{N+1}^2 - r_1^2\right)}{\sum_{i=1}^{N} R_{hyd,i}} \quad (7)$$

Equation (7) can be further simplified by considering only the most significant hydraulic resistance $R_{hyd,i}$ terms, which can generally be reduced to 1 or 2 depending on the design:

$$Q = \frac{\frac{1}{2}\rho\omega^2\left(r_{N+1}^2 - r_1^2\right)}{a+b} \quad (8)$$

From Eq. (8), only a and b terms have been retained and represent the two majors term contributing to the sum, while all the others $R_{hyd,j}$ have been neglected. First a term can be written as:

$$a = Max_{i=1}^{i=N}(R_{hyd,i}) = R_{hyd,j} = \frac{32\mu L_j}{h_j w_j D_{h,j}^{2.}} \qquad (9)$$

where (h_j, w_j) represent the height and the width of the S_j rectangular channel cross section, section extended along L_j channel length. $D_{h,j}$ represents the equivalent cylinder channel displaying a D_h diameter of S_j rectangular channel cross section (D_h was detailed in equation (2)), and μ is fluid viscosity.

1.2 Pinch valves

In order to account for the efficacy of the additional weakening structures, we performed a static analysis of the pinch valve deformation by using the Solid Mechanics module from the commercial software Comsol Multiphysics version 4.3 and a linear material model. As a test system we considered a pinch valve featuring a microchannel of $200\ \mu m$ width and $100\ \mu m$ height fabricated in a sheet of $500\ \mu m$ thick styrenics TPE material with mass density of $0.91\ g/cm^3$, Young elasticity modulus of $0.8\ MPa$ and a Poisson ratio of 0.45 that is bonded to a thin and rigid substrate (fixed boundaries). Additional weakening structures in the form of large and deep cavities placed symmetrically on both sides of the valve microchannel have been considered as well. Due to the symmetry of the problem, only half of the cross-sectional plane of the valve is taken into account in the computational domain (Fig. 1SIa). The compression exerted on the material from the actuation piston is modeled as a prescribed displacement (indicated by arrows in Fig. 1SIa) while all other boundaries except the contact with the rigid substrate are considered as free. Pressure at the boundary representing the piston is monitored for different values of prescribed displacements and the opening of the channel evaluated by computing the cross-sectional area of the channel at each displacement step. Since our model is limited to linear materials, only deformation steps up to the point where floor and ceiling of the microchannel are contacting each other are considered. Fig. 1SIb), c) and d) are three examples of such deformations for different applied pressures. The effect of adding weakening structures is illustrated in Fig. 1SIe, where applied pressure dependence of the openness of the channel is compared against two weakened configurations with $h = 200\ \mu m$ and $h = 500\ \mu m$ for the depth of the additional features. As we can see in this figure, the pressure necessary to close the microchannel can be reduced by about 20% by considering weakening cavities. However, the influence of their depth seems to be insignificant. This can be explained by the fact that the most part of the load is actually undertaken by two regions as illustrated in Fig. 1SIf, I) the peripheral region underneath the actuation piston but outside the weakening cavity and II) the region between the valve microchannel and the weakening cavities. Possible optimizations of the valve must consider then reductions in size for both these regions by matching the piston diameter to the actual size of the wakening structures and bring these structures as close as possible to the pinched microchannel. However, some limitations have to be considered in the later case since weakening cavities placed too close to the valve microchannel can cause eventual detachments of the TPE sheet from the bonding substrate and irreversibly affect the sealing of the microchannel when the valve is released.

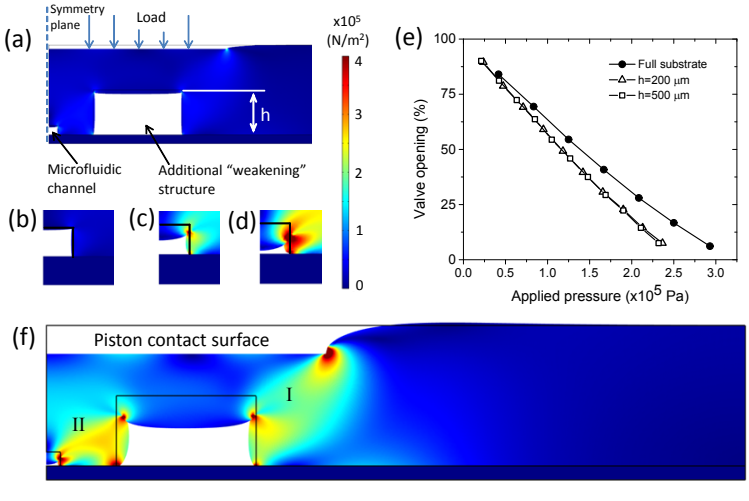

Figure 1SI Numerical study of the elastic deformation for a pinch microvalve fabricated in TPE : a) deformation and contour fill plot of von Mises stresses when an additional weakening structure of height h is employed; b-d) zoom in to the actual deformation of the microfluidic channel for an applied pressure of , and , respectively; e) Dependence of the microchannel valve opening on applied pressure for three types of valves: with additional weakening structures of (empty triangles) and (empty rectangles) height as well as without any additional features (full circles); f) Full view of the von Mises stresses in the computational domain

1.3 Fabrication and assembly

Classical photolithography was employed to fabricate the brittle SU–8 initial master structure, which was then transferred into a PDMS mold by soft lithography. Using a casting protocol over the resulting PDMS structure, an epoxy mold capable of withstanding the harsh process conditions associated with the thermal polymer replication by either hot embossing or injection molding technologies was obtained. The epoxy mold was obtained by mixing at 65 ^{o}C the two epoxy material components, the resin FR–1080 Conapoxy® and the Conacure® hardener at a ratio of 100/83 by weight (Cytec Corp, Woodland Park, NJ). The composition was poured onto the PDMS substrate and cured for 12 h at 80 ^{o}C. After curing, the PDMS was peeled-off, and a final annealing step of 2 h at 120 ^{o}C was performed. Subsequently, TPE sheet was placed on the epoxy mold and a Si wafer treated with an anti-adhesive layer was positioned on the top of the TPE. Embossing was performed under a primary vacuum at 135 ºC, under an applied force of 1.0 kN for 5 min (figure 2SI). With the force still applied, the system was cooled to 85 ºC, followed by the removal of the stack from the instrument and de-embossing of the TPE sheet.

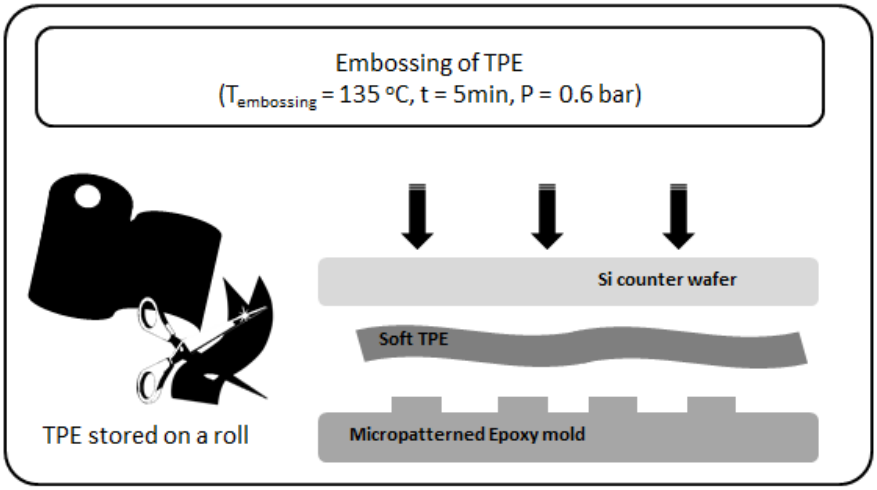

Figure 2SI Schematic illustration of the hot embossing process for the microstructuration of TPE substrate. TPE material has been extruded on a roll and can be store and use on demand.

The four microfluidic TPE hybridization component units were fabricated in the same manner and the final shaping of all TPE components was accomplished with a dedicated cutter/puncher tool for the precise definition of the CD shape and through-hole structures. The bottom CD substrate consisted of polycyclo-olefin (PCO) material (Zeonor 1060R, Zeon Chemicals, Louisville, KY) fabricated in the form of flat disks (120 mm in diameter, 0.25 mm in thickness) using an Engel e-motion 100 T injection molding tool (Engel Inc., Schwertberg, Austria). Four top flat DNA micro-array PCO components were fabricated using a Battenfled Microsystem50 injection molding (Wittmann-*Battenfeld* Inc. Kottingbrunn, *Austria*) and finally spotted with specific

oligomers (Integrated DNA Technologies, Inc., Coralville, Iowa) following the procedure earlier published.[5] Prior to the bonding and the assembly, reagents and magnets were dispensed into specific CD units (see section 2.4). Next, the mechanical properties of the TPE promoted an intimate contact of the CD with the thin PCO substrate, leading to perfect but reversible seal of the two thermoplastic surfaces. To achieve permanent bonding, a heating step of 70 ºC for 2 hours in a simple oven was applied. Finally, TPE hybridization chambers were placed on the top of the CD with the four spotted PCO micro-array components manually aligned and positioned over the hybridization chambers. Soft and sticky TPE material ensured good bonding of the sandwiched CD-chamber-microarray components.

1.4 Integration of liquid solution and solid reagents on the CD

Table 1SI lists all the details for the reagents and solution compositions involved in the assay at different levels. For example, a ratio of 10-lysate/10-PCR/4-exonuclease corresponds to the contact angle at the V_5 valve level, and describes the composition of the solution contained in the exonuclease unit. These measured values allowed us to calculate and fabricate the desired burst frequency for the liquid held in the operating unit prior to its downstream transfer.

	$\theta_{rec.}$		$\theta_{stat.}$		$\theta_{adv.}$	
	TPE	*PCO*	*TPE*	*PCO*	*TPE*	*PCO*
Lysate/PCR 10:10 ratio	56 ± 3	84 ± 3	104 ± 2	91 ± 1	114 ± 3	104 ± 1
PCR buffer	-	-	57 ± 4	31 ± 1	77 ± 1	46 ± 1
Lysate/PCR 10:10 ratio	27 ± 4	-	70 ± 6	34 ± 6	84 ± 4	45 ± 1
Exonuclease	49 ± 3	61 ± 5	81 ± 2	78 ± 5	101 ± 1	86 ± 1
Lysate/PCR/Exonuclease 10:10:4 ratio	-	-	30 ± 3	23 ± 2	46 ± 3	67 ± 3
Washing Buffer	24 ± 3	-	49 ± 2	41 ± 4	62 ± 1	63 ± 5

Table 1SI Measurements of receding $\theta_{rec.}$, static $\theta_{stat.}$ and advancing $\theta_{adv.}$ contact angles on Zeonor 1060R and styrenic TPE materials for different reagents and solutions involved in the assay.

2. Results and discussion

2.1 CD fabrication and characterization

Figures 5d-f show the scanning electron microscope images of the embossed CD featuring different structures with heights of 800, 100 and 20 µm. These images demonstrate well-defined shapes and excellent surface quality of the embossed structures. The surface roughness parameter Ra was measured to be 20± 2 nm and 25± 2 nm for the portions of the sample corresponding to un-patterned surface and microfluidic channel, respectively. Uniform and faithful motif replication over the entire CD area was observed, and the mold was used repeatedly more than 40 times, without any damages. The stability of the epoxy mold over repeated embossing runs, can also be contributed to easy de-moulding of the TPE due to its elastomeric properties (Young modulus of 1.75 ± 0.02 MPa at room temperature). Table 2SI displays the pitch size and depth measurements of different structures and reveals the shrinkage effects of the embossed TPE channels (measurements have been normalized to 100 and were related to aspect ratio structures of 1.0). The measured width and depth after first molding corresponded to 92.5 and 101.5 µm, respectively, yielding in-plane and out-plane shrinkage coefficients of 3.1% and 1.7%. For the twentieth embossing, these coefficients slightly increased to 3.3 and 2.6%. Shrinkage anisotropy was also evaluated, and a deviation ranging from 20 to 30 µm was characterized over the external CD diameter (D = 120 mm), yielding an anisotropic shrinkage coefficient of 0.03 to 0.05%. Finally, the selected soft TPE material is mainly amorphous and thus less prone to thermal shrinkage in comparison with crystalline and semi-crystalline materials. Table 2SI displays the pitch size and depth measurements of different structures and reveals the shrinkage effects of the embossed TPE

	SU-8	*PDMS*	*Epoxy*	*TPE n°1*	*TPE n°20*
Channel width (µm)	100	98.5	95.5	92.5	92.2
Channel height (µm)	100	99.1	104.3	102.5	101.5
Channel roughness(nm)	2 - 4	2 - 5	10 - 20	20 - 30	20 - 30
Anisotropy (%)	-	0.02	0.02	0.03	0.03

Table 2SI Successive shrinkage properties and characterization along each microfabrication step, including the initial photolithography step (SU–8), the soft lithography (PDMS), the epoxy mold fabrication (epoxy) and the CD TPE molding. The characterization of surface roughness of the fabricated parts and shrinkage anisotropy were investigated using atomic force microscopy and optical profilometery.

---

1 J. M. Chen, P.-C. Huang and M.-G. Lin, *Microfluid. Nanofluid.*, 2007, **4**, 427–437.

2 T.-S. Leu and P.-Y. Chang, *Sens. and Actuators A*, 2004, **115**, 508–515.

3 H. Cho, H.-Y. Kim, J. Y. Kang and T. S. Kim, *J. Colloid. Interf. Sci.*, 2007, **306**, 379–385.

4 M. Madou and G. Kellogg, *in Proc. SPIE Systems and Technologies for Clinical Diagnostics and Drug Discovery*, ed. G. E. Cohn and A. Katzir, San Jose, CA. USA, 1998, 80–93.

5 G. A. Diaz-Quijada, R. Peytavi, A. Nantel, E. Roy, M. G. Bergeron, M. M. Dumoulin and T. Veres, *Lab Chip*, 2007, **7**, 856–862.